The effect of nonlocal potential on the 14 N(p, γ) 15 O reaction cross section at low energies

Nguyen Hoang Phuc^{1,2,*}, Do Cong Cuong³, Nguyen Tri Toan Phuc^{4,2}



Use your smartphone to scan this QR code and download this article

¹Department of Applied Physics, Faculty

University of Technology (HCMUT), 268 Ly Thuong Kiet Street, Dien Hong Ward,

of Applied Science, Ho Chi Minh City

²Vietnam National University Ho Chi

Minh City, Linh Xuan Ward, Ho Chi

³Institute for Nuclear Science and

Technology, 179 Hoang Quoc Viet, Nghia Do, Hanoi, Vietnam

of Physics and Engineering Physics,

Nguyen Hoang Phuc, Department of

Applied Physics, Faculty of Applied

Kiet Street, Dien Hong Ward, Ho Chi

Science, Ho Chi Minh City University of Technology (HCMUT), 268 Ly Thuong

⁴Department of Nuclear Physics, Faculty

University of Science, Ho Chi Minh City,

Ho Chi Minh City, Vietnam

Minh City, Vietnam

Vietnam

Correspondence

Minh City, Vietnam

ABSTRACT

Introduction: The astrophysically crucial $^{14}N(p,\gamma)^{15}O$ reaction governs the carbon-nitrogenoxygen (CNO) cycle rate. Reliable theoretical predictions of this reaction require careful consideration of nuclear interactions. This study examines the influence of potential nonlocal effects on the calculated astrophysical S-factor for this reaction at low energies.

Methods: The calculable R-matrix method was applied within the potential model framework to calculate the S-factor of the $^{14}N(p,\gamma)^{15}O$ reaction. Results obtained with a local Woods-Saxon (WS) potential were compared with those from a nonlocal Perey-Buck (PB) potential.

Results: Although both models reproduced the experimental data reasonably well, the nonlocal potential required a ~12.5% smaller spectroscopic factor for normalization. Importantly, when extrapolated to zero energy, the S-factor in the nonlocal potential case was around 14% higher than in the local potential case.

Conclusion: The significant difference in the zero-energy S-factor observed in this study indicates that potential nonlocality effects are non-negligible and must be considered for accurate calculations of the $^{14}N(p,\gamma)^{15}O$ reaction rate in stellar environments.

Key words: CNÖ cycle in stars, radiative proton capture reaction (p, γ), calculable R-matrix, local potential, nonlocal potential.

INTRODUCTION

Radiative proton capture (p, γ) reactions are fundamental processes in stellar environments, providing the outward pressure that counteracts gravitational collapse and playing an essential role in nucleosynthesis ¹. In particular, these reactions serve as critical links within carbon-nitrogen-oxygen (CNO) cycles, which are the primary mechanism by which hydrogen burns into helium in stars more massive than the Sun. Figure 1 provides a schematic overview of the three principal CNO cycles operating within stars.

Due to their astrophysical significance, (p, γ) reaction rates have been a major focus of research into nuclear astrophysics. Extensive experimental efforts have aimed to measure these rates with high precision, providing crucial data for understanding stellar evolution and determining the cosmic abundances of the elements $^{2-4}$.

two primary mechanisms: capture via resonant states or direct capture (DC) into bound states. In particular, the DC process often dominates in reactions involving light nuclei at astrophysical energies. Describing the DC mechanism, especially in the low-energy regime relevant to stellar burning,

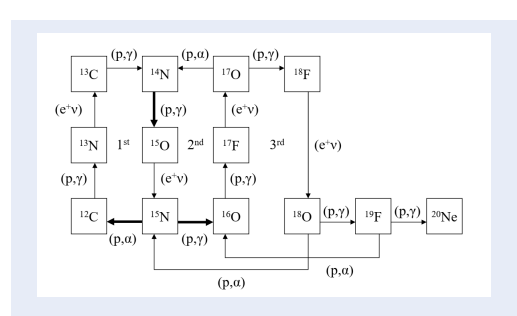


Figure 1: The first, second and third CNO cycles in

Proton capture reactions generally proceed through

requires reliable theoretical models. Current theoretical models for these reactions generally fall into two main categories: phenomenological R-matrix approaches 5-7 and microscopic calculations 8,9. The R-matrix method provides an effective parameterization of reaction data using resonance properties and asymptotic normalization coefficients (ANCs), while microscopic models, including ab initio and cluster models, aim to describe the reaction dynamics from fundamental nucleon degrees of freedom. Both methodologies offer distinct advantages and remain widely employed.

Vietnam National University Ho Chi Minh City, Linh Xuan Ward, Ho Chi Minh City, Vietnam

Email: nguyenhoangphuc@hcmut.edu.vn

Cite this article: Hoang Phuc N, Cong Cuong D, Tri Toan Phuc N. The effect of nonlocal potential on the 14 N(p, γ) 15 O reaction cross section at low energies. Sci. Tech. Dev. J. 2025; 28(4):3888-3895.

History

Received: 12-04-2025Revised: 08-08-2025Accepted: 19-09-2025Published Online: 01-12-2025

DOI:

https://doi.org/10.32508/stdj.v28i4.4453



Copyright

© VNUHCM Press. This is an openaccess article distributed under the terms of the Creative Commons Attribution 4.0 International license.



Bridging these two extremes is the potential model ^{3,4,8}, a widely used framework in nuclear astrophysics. In this approach, the DC cross section is determined by the interaction potential between the incident proton and the target nucleus. The potential model offers flexibility while maintaining a connection to microscopic physics through its consideration of nuclear potential.

A key aspect of the nuclear potential is its inherent nonlocality. In principle, the interaction depends not only on the relative coordinates of the colliding particles but also on their internal coordinates; it also exhibits energy dependence. This nonlocality arises primarily from the Pauli exclusion principle (antisymmetrization) as well as couplings between different reaction channels 10-14. Although this had been recognized even in the early days of nuclear physics 10,11, the implications of nonlocality have received renewed attention in recent years. Numerous studies have investigated nonlocal effects in a wide variety of reactions, including neutron transfer $(d, p)^{12,14,15}$, elastic scattering $^{16-21}$, and radiative nucleon capture 10,22,23. This study builds upon previous research to investigate the influence of potential nonlocality on a key astrophysical process: the $^{14}N(p,\gamma)^{15}O$ proton capture reaction at low energies, analyzed within the potential model

The $^{14}N(p,\gamma)^{15}O$ reaction is particularly important as it is the slowest reaction in the primary CNO cycle; consequently, it controls the overall energy generation rate and nucleosynthesis flow through this cycle. The first comprehensive experimental study of this reaction was performed in 1987 by Schroeder et al. 24 , who measured cross sections down to $E_p=200~KeV$ and identified the crucial $E_R=260~keV$ resonance that dominates the reaction rate under many stellar conditions. More recent experiments have extended measurements to even lower energies, reaching $E_p\approx70~keV^{25}$.

Despite this progress, theoretical calculations remain crucial, especially for extrapolating the cross section down to the Gamow peak energies that are relevant for stellar hydrogen burning (typically below 70 keV). Previous potential model calculations for $^{14}N\left(p,\gamma\right)^{15}O$ have mainly used local approximations for the nuclear potential 4,26 . Consequently, extending these calculations to incorporate nonlocal potentials while also systematically evaluating the impact of nonlocality on the predicted cross section is both relevant and timely. This study addresses this gap and provides a detailed analysis of the $^{14}N\left(p,\gamma\right)^{15}O$ reaction using both local and nonlocal potentials within the calculable R-matrix framework.

COMPUTATIONAL METHODS

Potential model

This section briefly outlines the formalism used to calculate the direct radiative capture cross section for the $A(p,\gamma)B$ reaction. The cross section is obtained by summing the partial cross sections over all relevant transitions from the initial scattering states $|J_iM_i\rangle$ to the final bound states $|J_fM_f\rangle$ [4,10,22,23,26]

$$\begin{split} &\sigma(E) = \sum_{\lambda, J_{i}, j_{f}} \sigma_{\lambda, j_{i} \to j_{f}}(E) \quad (1) \\ &\sigma_{\lambda, j_{i} \to j_{f}}(E) = \frac{4\pi(\lambda + 1)(2\lambda + 1)}{\lambda[(2\lambda + 1)!!]^{2}} \frac{\mu c^{2}}{(hc)^{2}} C_{\lambda}^{2} \frac{(2j_{i} + 1)(2j_{f} + 1)}{(2S + 1)} S_{F} \\ &\times \sum_{l_{i}j_{i}} i^{l_{i}} (-1)^{j_{f} + l_{f}} \widehat{J}_{i} \widehat{J}_{f} \widehat{l}_{f} \begin{cases} j_{i} & J_{i} & S \\ J_{f} & j_{f} & \lambda \end{cases} \begin{cases} l_{i} & j_{i} & \frac{1}{2} \\ j_{f} & lf & \lambda \end{cases} \\ \langle l_{i}0, \lambda 0 | l_{f} 0 \rangle I(k) \Big|^{2} \quad (2) \end{split}$$

where $\mu = m_A m_p / (m_A + m_p)$ is the reduced mass of the proton-target system, and m_A and m_D are the masses of the nucleus A and the proton, respectively. In addition, $C_{\lambda} = e \left[m_A^{\lambda} + Z_A \left(-m_p \right)^{\lambda} \right] / m_B^{\lambda}$ is the effective charge, Z_A is the target proton number, S is the spin of the target nucleus, and S_F is the spectroscopic factor of the bound state. $|J_i = l_i \pm 1/2|$ and $|J_i| = l_i \pm 1/2$ are the total angular momentum of the proton in its initial and final states, respectively, l_i and l_f are the orbital angular momentum of the proton in its initial and final states, respectively, where $\hat{j} = \sqrt{2j+1}.k = \sqrt{2\mu E}/h$ represents the wave numbers for the incident proton energy E and k_{γ} represents the wave numbers for the emitted photon energy E_{γ} . According to the potential model, I(k) is the radial overlap integral of the scattering wave function $\chi_{l_i j_i}(k,r)$ and the bound-state wave function $\phi_{n_f l_f j_f}(r)$ (where n_f is the number of nodes). It is given by the following equation:

$$I(k) = \int_0^\infty \phi_{n_f l_f j_f}(r) \chi_{l_i j_i}(k, r) r^{\lambda} dr$$
 (3)

The reaction cross section determined by Equation (1) decreases very rapidly as energy decreases due to the tunneling effect. It is thus therefore it is convenient to use the astrophysical S-factor instead: this quantity is related to the relates to the reaction cross section as follows:

$$S(E) = E \exp(2\pi\eta) \sigma(E) \quad (4)$$

where η is the Sommerfeld parameter.

In the potential model, the reaction cross section $\sigma(E)$ is determined throughout the scattering wave functions of the system in the initial state and the bound-state wave functions of the system in the final state. Both the bound-state and scattering wave functions in Equation (3) are solutions of the Schrödinger equation with the proton–nucleus interaction potential, which can be represented in either local or nonlocal form. Within the framework of the local potential, the Schrödinger equation has the form 4,26 :

$$\begin{split} &-\frac{h^{2}}{2\mu}\left[\frac{d^{2}}{dr^{2}}-\frac{l(l+1)}{r^{2}}\right]\psi_{lj}\left(k,r\right)+\\ &\left[V_{l}\left(r\right)+l\sigma V_{SO}\left(r\right)+V_{C}\left(r\right)\right]\psi_{lj}\left(k,r\right)\\ &=E\psi_{lj}\left(k,r\right)\;(5) \end{split}$$

where the solution $\psi_{lj}(k,r)$ for the case scattering state system (E>0) is denoted as $\chi_{l_lj_l}(r)$, and in a while the solution for a bound state system (E<0) is denoted as $\phi_{n_fl_fj_f}(r)$. $V_L(r)$, $V_{SO}(r)$ and $V_C(r)$ are respectively represent the central, spin-orbit, and local Coulomb potential components, respectively. The Coulomb potential component is determined as follows 4,26 .

$$V_C(r) = \begin{cases} \frac{Z_A e^2}{r}, & r > R_C \\ \frac{Z_A e^2}{2R_C} \left(3 - \frac{r^2}{R_C^2}\right), & r \le R_C \end{cases}$$
(6)

With where $R_C = 1.25A^{1/3}(fm)$ and A is the mass number of the target. The nuclear and spin-orbit potential components are typically presented using the phenomenological Woods-Saxon (WS) form as follows:

$$\begin{aligned} V_l\left(r\right) &= -V_0 f_c\left(r\right) \quad (7) \\ V_{SO}\left(r\right) &= \left(\frac{h}{m_\pi c}\right)^2 V_{0S} \frac{1}{r} \frac{d}{dr} f_{SO}\left(r\right) \quad (8) \end{aligned}$$

where $f_x(r) = \left[1 + exp\left(\frac{r - R_x}{a_x}\right)\right]^{-1}$, such that $x \equiv c$, SO, R_x and a_x are the radius and diffuseness of the WS potential, respectively. V_0 and V_{0S} are the strengths of the central and spin-orbit potentials, respectively. The spin-orbit interaction in Equation (8) is written in terms of the pion Compton wavelength with $\left(\frac{h}{m_x c}\right)^2 \approx 2$. In the nonlocal potential case, the central potential is typically presented in the Perey-Buck (PB) phenomenological form 11 ; in such cases, the Schrödinger equation is written as:

$$-\frac{h^{2}}{2\mu} \left[\frac{d^{2}}{dr^{2}} - \frac{l(l+1)}{r^{2}} \right] \psi_{lj}(k,r) + [l\sigma V_{SO}(r) + V_{C}(r)]$$

$$\psi_{lj}(k,r) + \int v_{l}(r,r') \psi_{lj}(k,r') dr' = E \psi_{lj}(k,r) \quad (9)$$
where $v_{l}(r,r')$ is the PB-type potential:

$$v_l(r,r') = U\left(\frac{r+r'}{2}\right) \frac{1}{\sqrt{\pi\beta}} exp\left[-\frac{\left(r^2+r'^2\right)}{\beta^2}\right]$$
$$2i^l z j_l(-iz) (10)$$

where U(x) has the WS form with $U(x) = V_{NL}f_c(x)$ and $z = 2rr'/\beta^2$, such that β is the nonlocality range, $j_l(x)$ is the spherical Bessel function, and V_{NL} is the strengths of the central potentials. In this study, only the central potential is treated as nonlocal; all other potential components are retained in the local form as described above.

For the scattering wave function, the asymptotic form of the scattering wave at large distances, where the nuclear potential $V \to 0$, is given by:

$$\chi_{l_i j_i}(k,r \to \infty) = [F_{l_i}(kr)\cos\delta_{l_i j_i}] \exp\left[i\left(\delta_{l_i}^c + \delta_{l_i j_i}\right)\right]$$
 (11) where G and F are the regular and irregular Coulomb functions, respectively²⁷, and $\delta_{l_i}^c$ and $\delta_{l_i j_i}$ are the Coulomb and nuclear phase shifts, respectively.

For a system in a bound state, the wave function asymptotically approaches the form of a Whittaker function $W_{-\eta,l_f+\frac{1}{2}}(x)^{28}$:

 $\phi_{n_f l_f j_f}(r) = b_{n_f l_f j_f} W_{-\eta, l_f + \frac{1}{2}}(2kr)$ with $r > R_m$ (12) where $b_{n_f l_f j_f}$ is the asymptotic amplitude of the bound-state wave function, known as the single-particle asymptotic normalization coefficient (ANC), $\kappa = \sqrt{-2\mu E_B}/h$ is the wave number of the bound state with $E_B < 0$ being the separation energy between the proton and the target nucleus A, and the radius R_m is chosen to be sufficiently large such that the nuclear potential for $r > R_m$ is negligible.

Calculable R-matrix method

In this study, the calculable R-matrix method 27 is used to solve the local (Equation 5) and nonlocal (Equation 9) Schrödinger equations. The calculable R-matrix method aims to divide the wave function into two regions, an internal region and an external region, separated at the channel radius $r = R_m$. The value of R_m is chosen to be large enough such that the nuclear interaction potential in the external region is zero. In such cases, the wave function in the internal region can be expanded linearly in terms of basis functions as follows:

$$\psi_{lj}^{int}\left(r\right) = \sum_{n=1}^{N} C_n \varphi_n\left(r\right)$$
 (13)

where $\varphi_n(r)$ is a set of basis functions. The wave functions in the internal and external regions must be continuous at $r = R_m$, which leads to the definition of the R-matrix at energy E as:

 $\psi_{lj}(R_m) = \mathfrak{R}_{lj}(E) \left[R_m \psi'_{lj}(R_m) - B \psi_{lj}(R_m) \right]$ (14) where B is a boundary parameter determined according to the specific case. Since the Hamilton operator is not guaranteed to be Hermitian in the internal region $(0, R_m)$, solving the Schrödinger equation is not trivial. This issue can be addressed by adding the Bloch operator as follows 27,29 :

$$L(B) = \frac{h^2}{2\mu} \delta(r - R_m) \left(\frac{d}{dr} - \frac{B}{r}\right)$$
 (15)
This results in a modified Hamiltonian operator that

This results in a modified Hamiltonian operator that satisfies Hermitian properties over $(0, R_m)$ with B being a real number.

For a system in a scattering state, the R-matrix in Equation (14) is independent of B. Consequently, B=0 can be used to simplify the calculation. The radial function of Equation (9) can thus be rewritten

$$\begin{cases} -\frac{h^2}{2\mu} \left[\frac{d^2}{dr^2} - \frac{l(l+1)}{r^2} \right] + V_C(r) + l\sigma V_{SO}(r) - E + L(0) \right\} \\ \sum_{n=1}^{N} C_n \varphi_n(r) + \int v_l(r,r') \sum_{n=1}^{N} C_n \varphi_n(r') dr' \\ = L(0) \psi_{lj}^{ext}(r) (16) \end{cases}$$
Where $\psi_{lj}^{ext}(r)$ is the wave function in the external re-

Where $\psi_{lj}^{ext}(r)$ is the wave function in the external region with $r \ge R_m$. Successively multiplying both sides of Equation (16) by the function $\varphi_i(r)$ and integrating

over the variable r, we obtain the following system of linear equations:

where the matrix element
$$C_{in}$$
 is determined as follows:
$$C_{in}(E,0) c_n = \frac{h^2}{2\mu} \varphi_i(R_m) \frac{d\psi_{ij}^{ext}(R_m)}{dr} \Big|_{r=R_m} (17)$$
where the matrix element C_{in} is determined as follows:
$$C_{in}(E,0) = \int \varphi_i(r) \left\{ -\frac{h^2}{2\mu} \left[\frac{d^2}{dr^2} - \frac{l(l+1)}{r^2} \right] + V_C(r) + l \sigma V_{SO}(r) - E + L(0) \right\}$$

 $\varphi_n(r) dr + \int \varphi_i(r) v_l(r,r') \varphi_n(r') dr dr'$ (18) Solving the system of equations in (17) allows for the determination of the coefficients c_n , from which the scattering wave function in the internal region can be obtained from Equation (13) while the R-matrix can be obtained from Equation (14) as follows:

 $\mathfrak{R}_{lj}(E) = \frac{h^2}{2uR_m} \sum_{i,n=1}^{N} \varphi_i(R_m) (C^{-1})_{in} \varphi_n(R_m)$ (19) In the external region, the wave function contains the scattering matrix element $S_{ij} = e^{2i\delta l_i j_i}$ while the internal region contains the R-matrix component $\mathfrak{R}_{li}(E)$. By applying the continuity condition of the wave function, the relationship between S_{lj} and $\mathfrak{R}_{lj}(E)$ can be established:

$$S_{lj}=e^{2i\phi_l}\frac{1-L_l^*\mathfrak{R}_{lj}(E)}{1-L_l\mathfrak{R}_{lj}(E)}~(20)$$
 where

$$L_{l} = \frac{kR_{m}}{O_{l}(kR_{m})} \frac{dO_{l}(kR_{m})}{dr} | r = R_{m}$$
 (21)

 $O_{l} = argI_{l}(kR_{m}) = -arc \tan \left[\frac{F_{l}(kR_{m})}{G_{l}(kR_{m})}\right] (22)$

is the phase shift for scattering off a hard sphere. Once S_{li} has been determined, the scattering wave function in the external region can also be determined from Equation (11).

For a bound-state system, the asymptotic form of the wave function follows Equation (12), and the boundary parameter B (Equation 15) can be chosen as fol-

$$B = S_l(E_B) = 2\kappa R_m \frac{W'_{-\eta, l+1/2}(2\kappa r)}{W_{-\eta, l+1/2}(2\kappa r)}$$
(23)

Hence, the matrix element C_{in} in Equation (17) becomes an eigenvalue problem

$$\sum_{n=1}^{N} C_{in}(E, B) c_n = 0 (24)$$

Since the boundary parameter B depends on the energy E, the solution can be found using an iterative method starting with B = 0 and iterating until E_B converges, allowing us to obtain the values of c_n from Equation (24). A normalization factor is introduced to satisfy the normalization condition of the boundstate wave function ²⁷:

State water takenships
$$N_l = 1 + \gamma_l^2 \left[\frac{dS_l(E_B)}{dE} \right]_{E=E_B}$$
 (25) where γ_l is the reduced width determined by:

$$\gamma_{l} = \left(\frac{h^{2}}{2\mu R_{m}}\right)^{1/2} \sum_{i,n=1}^{N} c_{n} \varphi_{n}(R_{m})$$
 (26)

 $\gamma_l = \left(\frac{h^2}{2\mu R_m}\right)^{1/2} \sum_{i,n=1}^N c_n \varphi_n\left(R_m\right)$ (26) and the internal wave function of the bound state given by Equation (13) can be rewritten as:

$$\psi_{lj}^{int}(r) = N_l^{-1/2} \sum_{n=1}^{N} c_n \varphi_n(r)$$
 (27)

The standard asymptotic coefficient is defined as:

$$b_{nlj} = \frac{N_l^{-1/2} \sum_{n=1}^{N} c_n \varphi_n(r)}{W \frac{1}{2 \kappa R_m} (2\kappa R_m)}$$
(28)

From this, the bound-state wave function in the external region can be determined according to Equation (12).

RESULTS

The $^{14}N(p, \gamma)$ ^{15}O reaction proceeds from the capture of a proton from a scattering state by the parent nucleus ¹⁴N, forming the bound state ¹⁵O while simultaneously emitting a gamma ray. The most comprehensive experiment measuring the $^{14}N(p,\gamma)^{15}O$ reaction was performed by Schroeder et al. 24 in 1987, with the incident proton energy measured down to $E_p = 200 \text{ keV}$. In this energy range, there are two resonance states in the scattering state that affect the reaction cross section: $E_{R1} \approx 260 \, keV \, \left(J_{R1}^{\pi} = 1/2^{+}\right)$ and $E_{R2} \approx 987 \ keV \ \left(J_{R2}^{\pi} = 3/2^{+}\right)^{24}$. Accurately determining the cross section of the $^{14}N(p,\gamma)^{15}O$ reaction requires the characterization of both of these resonance states as well as the final bound state.

The R1 resonance state has a spin and parity of $1/2^+$. In the simple configuration model, where the ¹⁴N core is coupled with a valence proton, this resonance state can exist in two configurations: $\left[I_c\otimes s_{1/2^+}\right]_{1/2^+}$ or $I_c \otimes d_{3/2^+} \Big|_{3/2^+}$, with core spin $I_c = 1^+$. Meanwhile, the bound state includes possible excited states and the ground state of 15 O.

In this study, we only consider the ground state of ¹⁵O, which has the configuration $\left|I_c \otimes p_{1/2^-}\right|_{1/2^-}$. Thus, there exist two possibilities for the E1 gamma transition from the R1 resonance state to the ground state of ¹⁵O: $|I_c \otimes s_{1/2^+}|_{1/2^+} \to |I_c \otimes p_{1/2^-}|_{1/2^-}$ and $[I_c \otimes d_{3/2^+}]_{1/2^+} \rightarrow [I_c \otimes p_{1/2^-}]_{1/2^-}$. ever, a recent study 30 showed that the second transition $\left[I_c \otimes d_{3/2^+}\right]_{1/2^+}^{\prime} \rightarrow \left[I_c \otimes p_{1/2^-}\right]_{1/2^-}^{\prime}$ contributes very little to the total cross section. fore, we only consider the E1 transition from $\begin{bmatrix} I_c \otimes s_{1/2^+} \end{bmatrix}_{1/2^+} \rightarrow \begin{bmatrix} I_c \otimes p_{1/2^-} \end{bmatrix}_{1/2^-}$

Similarly, the R2 state has a spin and parity of $3/2^+$. The two possible configurations for this state are $\left[I_c \otimes s_{1/2^+}\right]_{3/2^+}$ or $\left[I_c \otimes d_{3/2^+}\right]_{3/2^+}$. In this case, both configurations contribute significantly to the E1 transition from the resonance state to the ground state $\left\lfloor I_c \otimes p_{1/2^-} \right\rfloor_{1/2^-}$. Thus, this study investigated the transitions from both these resonance configurations to the ground state.

Table 1: The WS and PB parameters of the nuclear interaction potential used in the calculation of the
$^{14}N(p,\gamma)^{15}O$ cross section.

$E_{R1}\left(E_{B}\right)$ (MeV)	Potential	V_0 (MeV)	R_c (fm)	a_c (fm)	β (fm)	
Scattering state $s_{1/2}$ with $\left[I_c\otimes s_{1/2^+}\right]_{1/2^+}$ and $\left[I_c\otimes s_{1/2^+}\right]_{3/2^+}$						
0.260	Local	52.38	3.0828	0.65		
	Nonlocal	67.35	3.0828	0.65	0.85	
0.987	Local	45.38	3.0828	0.65		
	Nonlocal	57.60	3.0828	0.65	0.85	
Scattering state $d_{3/2}$ with $\left[I_c\otimes d_{3/2^+} ight]_{3/2^+}$						
0.987	Local	55.38	3.0828	0.65		
	Nonlocal	77.90	3.0828	0.65	0.85	
Bound state $p_{1/2}$ with $\left[I_c\otimes p_{1/2^-} ight]_{1/2^-}$						
7.297	Local	48.83	3.0828	0.65		
	Nonlocal	57.30	3.0828	0.65	0.85	

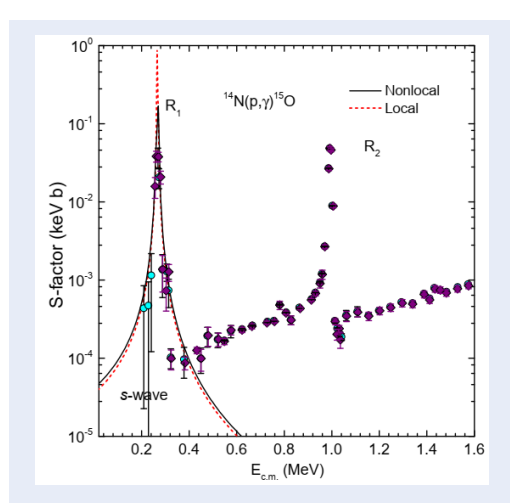


Figure 2: S-factor corresponding to the R1 resonance of the $^{14}N(p,\gamma)^{15}O$ reaction obtained from the calculable R-matrix method employing phenomenological local WS and nonlocal PB potentials. The solid line represents the result of the calculation with the nonlocal PB potential, while the dashed line represents the result of the calculation with the local WS potential. Experimental data were taken from 24 31 .

To describe the resonance states R1, R2 and the bound state of 15 O, the potential radius and diffuseness parameters for the central and spin-orbit potential components were fixed at $R=1.25A^{1/3}$ fm and $\alpha=0.65$ fm. The strength of the spin-orbit potential was also held constant at $V_{os}=5$ MeV. It is worth noting that the contribution of the spin-orbit

term is negligible compared to the central component; consequently, it is sometimes omitted for computational simplicity 4 . There was an additional nonlocality range parameter $\beta=0.85~fm$ for the nonlocal potential case.

The strength of the central potential component was treated as a free parameter that was adjusted to match the resonance energies of the scattering states $E_{R1} \approx 260 \ keV$, $E_{R2} \approx 987 \ keV$, and the separation energy of the valence proton from the 14 N core in the 15 O ground state, $E_B = 7.297 \ MeV$. The resulting parameter values for the local WS and nonlocal PB potentials are presented in Table 1. From these parameters, the scattering and bound-state wave functions were determined using the R-matrix method with a channel radius of $R_m = 15 \ fm$.

Based on experimental data for the reaction cross section, the spectroscopic factor of the $^{15}{\rm O}$ bound state in the ground state was found to be $S_F=0.004$ for the local potential case and $S_F=0.0035$ for the nonlocal potential case. The calculated S-factor results for the R1 resonance peak are shown in Figure 2. As previously mentioned, only the E1 transition from the $s_{1/2}$ wave state to $p_{1/2}\left(\left[I_c\otimes s_{1/2^+}\right]_{1/2^+}\rightarrow\left[I_c\otimes p_{1/2^-}\right]_{1/2^-}\right)$ was considered for this case. It was found that the S-factors corresponding to the nonlocal and local potentials were almost identical at the resonance peak. However, in the resonance tail, the S-factor corresponding to the nonlocal potential case was found to

be higher than the local potential case by about 14%.

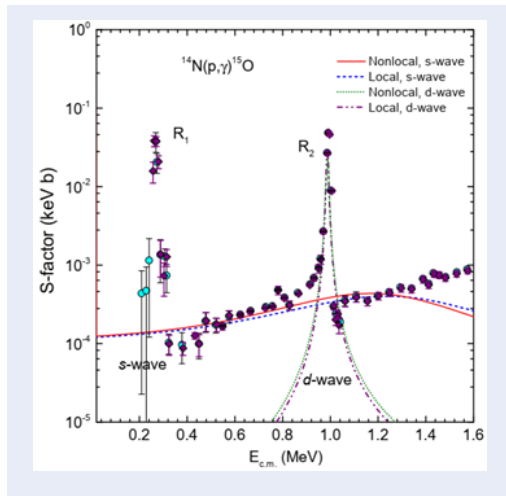


Figure 3: S-factor corresponding to the R2 resonance of the $^{14}N(p,\gamma)^{15}O$ reaction. All other elements of this graph are identical to Figure 2.

In the case of R2 resonance, there are two E1 transitions: from the $s_{1/2}$ wave state to $p_{1/2}\left(\left[I_c\otimes s_{1/2^+}\right]_{3/2^+} \to \left[I_c\otimes p_{1/2^-}\right]_{1/2^-}\right)$ and from the $d_{3/2}$ state to

and from the
$$d_{3/2}$$
 state $p_{1/2}\left(\left[I_c\otimes d_{3/2}+\right]_{3/2^+}\to \left[I_c\otimes p_{1/2^-}\right]_{1/2^-}\right).$

The R2 resonance peak is primarily dominated by the $d_{3/2}$ wave state to $p_{1/2}$ transition. Indeed, the $s_{1/2}$ state to $p_{1/2}$ transition mostly plays a background role, fitting experimental points outside the R2 resonance peak. The calculated S-factor for the R2 resonance case is presented in Figure 3. Like the R1 resonance case, the S-factor corresponding to the R2 resonance peak for the transition from $d_{3/2}$ to $p_{1/2}$ was found to be identical in for both the local and nonlocal potentials. However, in the resonance tail, the S-factor corresponding to the nonlocal potential case was larger than the local potential case by about 20%. There were small S-factor differences for the transition from the $s_{1/2}$ state to $p_{1/2}$ in the energy range $E_{c.m.}$ between 0.6 and 1.6 MeV. The total S-factor of these two peaks is presented in Figure 4.

DISCUSSION

The WS and PB potential parameters obtained in this study (Table 1) were relatively similar to the families of local and nonlocal potentials previously used to study (p, γ) reactions for light nuclei 10,22,23,26 . In general, the nonlocal potential tends to be deeper than the local potential for the same nuclear state. In phenomenological models such as Perey–Buck 11 , explicitly including nonlocality requires a deeper central

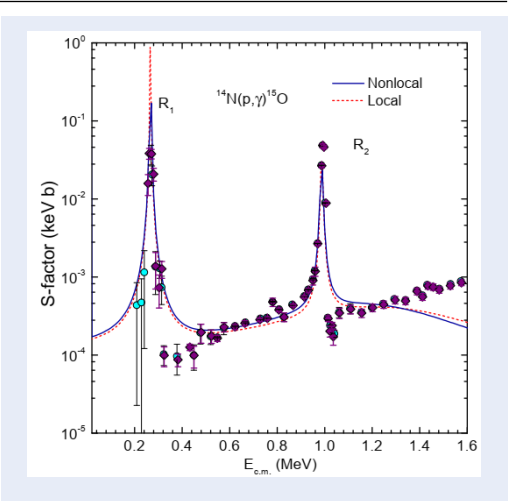


Figure 4: Total S-factor of the $^{14}N(p,\gamma)^{15}O$ reaction as calculated using the calculable R-matrix method employing phenomenological local WS and nonlocal PB potentials. The solid line represents the result of the calculation with the nonlocal PB potential, while the dashed line represents the result of the calculation with the local WS potential. Experimental data were taken from 24,31 .

potential to counteract the Perey effect, which suppresses the wave function amplitude in the nuclear interior and effectively weakens the interaction. This adjustment ensures that scattering observables remain consistent with the physical role of nonlocality, while still properly accounting for many-body correlations without overcounting the Pauli-forbidden states

Figure 4 shows that local and nonlocal interaction potential models can accurately describe the experimental data at two key resonance peaks ($E_{R1} \approx 260 \ keV$ and $E_{R2} \approx 987 \ keV$). In order to fit the experimental data, the spectroscopic factor for the nonlocal potential case must be smaller than the local potential case by about 12.5%. A smaller spectroscopic factor implies that the tail of the bound-state wave function in the nonlocal potential case tends to be larger than in the local potential case. It is also important to note that the spectroscopic factor S_F obtained from fitting the resonant (p, γ) reaction is not directly comparable to the spectroscopic factors derived from nuclear structure models or from experimental knockout and transfer reactions. For instance, shell-model calculations yield $S_F = 1.6$ for the $p_{1/2}$ valence proton state in the 15 O ground state 32,33 , while the $^{15}O(p,2p)$ ^{14}N knockout reaction experiment found that $S_F \approx 1.22$ at energies below 100 MeV/nucleon [33] and that $S_F \approx 1.68$ at 310 MeV/nucleon³⁴. These values are significantly larger than the S_F obtained from fitting the $^{14}N(p,\gamma)^{15}O$ reaction for the R1 and R2 resonances.

The resonance tail near zero energy plays a critical role in determining the reaction rate of $^{14}N(p,\gamma)$ ^{15}O in stellar environments. Although the resonance peak data can be well-described by both local and nonlocal potentials, Figure 4 shows that the S-factor in the resonance tail is higher in the nonlocal potential case than in the local potential case. Indeed, the difference in the astrophysical S-factor at near-zero energy between the nonlocal and local potentials is 14%. This is a significant difference, demonstrating that nonlocal effects must be seriously considered during the calculation of the cross section (or S-factor) for the $^{14}N(p,\gamma)$ ^{15}O reaction.

CONCLUSIONS

This study investigates the $^{14}N(p,\gamma)^{15}O$ reaction cross section near astrophysically relevant energy regions within the framework of the interaction potential model using the calculable R-matrix method. Calculations with local and nonlocal potentials show that, to match the experimentally derived (p,γ) reaction cross section data, the spectroscopic factor of the local potential case is always larger than for the nonlocal potential case by 12.5%. Furthermore, at near-zero energies, the astrophysical S-factor obtained from the nonlocal potential calculation is 14% larger than that from the local potential. These results demonstrate that the nonlocal effect cannot be ignored during S-factor calculation for the $^{14}N(p,\gamma)^{15}O$ reaction.

Only the nonlocal effect of the phenomenological PB potential was considered. An extension of this study, which involves more microscopic models of nonlocal potential calculation, is currently underway. These findings serve as a foundation for further studies on nonlocal effects in other (p,γ) reactions within the CNO cycle.

LIST OF ABBREVIATIONS

CNO: Carbon-Nitrogen-Oxygen

WS: Woods-Saxon PB: Perey-Buck DC: Direct capture

ANC: Asymptotic Normalization Coefficient

COMPETING INTERESTS

The authors declare that they have no conflicts of interest.

AUTHORS' CONTRIBUTIONS

Nguyen Hoang Phuc and Do Cong Cuong performed the calculations; Nguyen Hoang Phuc and Do Cong Cuong prepared the manuscript; Nguyen Tri Toan Phuc discussed the results and revised the manuscript.

ACKNOWLEDGEMENTS

We thank Dao Tien Khoa for his enlightening discussions.

REFERENCES

- Iliadis C. Nuclear physics of stars. Weinheim: Wiley-VCH Verlag GmbH; 2007. Available from: https://doi.org/10.1002/ 9783527618750.
- Adelberger EG, García A, Robertson RG, Snover KA, Balantekin AB, Heeger K, et al. Solar fusion cross sections. II. The pp chain and CNO cycles. Rev Mod Phys. 2011;83(1):195–245. Available from: https://doi.org/10.1103/RevModPhys.83.195.
- Angulo C, Arnould M, Rayet M, Descouvement P, Baye D, Leclercq-Willain C, et al. A compilation of charged-particle induced thermonuclear reaction rates. Nucl Phys A. 1999;656(1):3–183. Available from: https://doi.org/10.1016/S0375-9474(99)00030-5.
- Xu Y, Takahashi K, Goriely S, Arnould M, Ohta M, Utsunomiya H. NACRE II: an update of the NACRE compilation of chargedparticle-induced thermonuclear reaction rates for nuclei with mass number A<16. Nucl Phys A. 2013;918:61–169. Available from: https://doi.org/10.1016/j.nuclphysa.2013.09.007.
- Wigner E. Resonance reactions and anomalous scattering. Phys Rev. 1946;70(1-2):15–33. Available from: https://doi.org/ 10.1103/PhysRev.70.15.
- Wigner EP, Eisenbud L. Higher angular momenta and long range interaction in resonance reactions. Phys Rev. 1947;72(1):29–41. Available from: https://doi.org/10.1103/ PhysRev.72.29.
- Descouvement P. Nuclear reactions of astrophysical interest. Front Astron Space Sci. 2020;7:9. Available from: https://doi. org/10.3389/fspas.2020.00009.
- Barrett BR, Navrátil P, Vary JP. Ab initio no core shell model. Prog Part Nucl Phys. 2013;69:131–81. Available from: https://doi.org/10.1016/j.ppnp.2012.10.003.
- Wildermuth K, Tang YC. A unified theory of the nucleus. Braunschweig: Vieweg; 1977. Available from: https://doi.org/10. 1007/978-3-322-85255-7.
- Tian Y, Pang DY, Ma ZY. Effects of nonlocality of nuclear potentials on direct capture reactions. Phys Rev C. 2018;97(6).
 Available from: https://doi.org/10.1103/PhysRevC.97.064615.
- Perey F, Buck B. A non-local potential model for the scattering of neutrons by nuclei. Nucl Phys. 1962;32:353–80. Available from: https://doi.org/10.1016/0029-5582(62)90345-0.
- Titus LJ, Nunes FM, Potel G. Explicit inclusion of nonlocality in (d,p) transfer reactions. Phys Rev C. 2016;93(1). Available from: https://doi.org/10.1103/PhysRevC.93.014604.
- Loan DT, Phuc NH, Khoa DT. R-matrix method and the nonlocal nucleon optical potential. Commun Phys. 2018;28(4):323. Available from: https://doi.org/10.15625/ 0868-3166/28/4/12760.
- Timofeyuk NK, Johnson RC. Nonlocality in deuteron stripping reactions. Phys Rev Lett. 2013;110(11). Available from: https://doi.org/10.1103/PhysRevLett.110.112501.
- Li W, Potel G, Nunes F. Nonlocal interactions in the (d,p) surrogate method for (n,γ) reactions. Phys Rev C. 2018;98(4). Available from: https://doi.org/10.1103/PhysRevC.98.044621.
- Jaghoub MI, Lovell AE, Nunes FM. Exploration of the energy dependence of proton nonlocal optical potentials. Phys Rev C. 2018;98(2). Available from: https://doi.org/10.1103/PhysRevC. 98.024609.
- Mahzoon MH, Charity RJ, Dickhoff WH, Dussan H, Waldecker SJ. Forging the link between nuclear reactions and nuclear structure. Phys Rev Lett. 2014;112(16). Available from: https: //doi.org/10.1103/PhysRevLett.112.162503.

- Minomo K, Ogata K, Kohno M, Shimizu YR, Yahiro M. Brieva-Rook localization of the microscopic nucleon-nucleus potential. J Phys G Nucl Part Phys. 2010;37(8). Available from: https://doi.org/10.1088/0954-3899/37/8/085011.
- Minomo K, Washiyama K, Ogata K. Reexamination of microscopic optical potentials based on multiple scattering theory. 2017;.
- Loan DT, Khoa DT, Phuc NH. Rearrangement term in the folding model of the nucleon optical potential. J Phys G Nucl Part Phys. 2020;47(3). Available from: https://doi.org/10.1088/ 1361-6471/ab5f54.
- 21. Khoa DT, Loan DT, Phuc NH. Pauli nonlocality and the nucleon effective mass. Phys Rev C. 2024;110(2). Available from: https://doi.org/10.1103/PhysRevC.110.024607.
- Phuc NH, Phuc NT, Cuong DC. Study of nonlocality effects in direct capture reactions with Lagrange-mesh R-matrix method. Int J Mod Phys E. 2021;30(9). Available from: https://doi.org/10.1142/S0218301321500798.
- Anh NL, Phuc NH, Khoa DT, Chien LH, Phuc NT. Folding model approach to the elastic p+12,13C scattering at low energies and radiative capture 12,13C(p, γ) reactions. Nucl Phys A. 2021;1006. Available from: https://doi.org/10.1016/j. nuclphysa.2020.122078.
- Schroder U, Becker HW, Bogaert G, Görres J, Rolfs C, Trautvetter HP, et al. Stellar reaction rate of 14N(p, γ)15O and hydrogen burning in massive stars. Nucl Phys A. 1987;467(2):240–60.
 Available from: https://doi.org/10.1016/0375-9474(87)90528-8.
- Lemut A, Bemmerer D, Confortola F, Bonetti R, Broggini C, Corvisiero P, et al. First measurement of the 14N(p, γ)15O cross section down to 70 keV. Phys Lett B. 2006;634(5-6):483–7. Available from: https://doi.org/10.1016/j.physletb.2006.02.021.
- Huang JT, Bertulani CA, Guimarães V. Radiative capture of nucleons at astrophysical energies with single-particle states.

- At Data Nucl Data Tables. 2010;96(6):824–47. Available from: https://doi.org/10.1016/j.adt.2010.06.004.
- Descouvement P, Baye D. The R-matrix theory. Rep Prog Phys. 2010;73(3). Available from: https://doi.org/10.1088/ 0034-4885/73/3/036301.
- Abramowitz M, Stegun IA. Handbook of mathematical functions with formulas, graphs, and mathematical tables. and others, editor. Washington, DC: US Government Printing Office: 1972.
- Bloch C. Une formulation unifiée de la théorie des réactions nucléaires. Nucl Phys. 1957;4:503–28. Available from: https: //doi.org/10.1016/0029-5582(87)90058-7.
- Anh NL, Loc BM, undefined Nguyen Le Anh, undefined Bui Minh Loc. Bound-to-continuum potential model for the (p, γ) reactions of the CNO nucleosynthesis cycle. Phys Rev C. 2021;103(3). Available from: https://doi.org/10.1103/ PhysRevC.103.035812.
- Formicola A, Costantini H, Imbriani G. A new study of the 14N(p,y)15O reaction at low energy. Nucl Phys A. 2003;94C:719. Available from: https://doi.org/10.1016/S0375-9474(03)00974-6.
- Warburton EK, Brown BA. Effective interactions for the 0p1s0d nuclear shell-model space. Phys Rev C Nucl Phys. 1992;46(3):923–44. Available from: https://doi.org/10.1103/ PhysRevC.46.923.
- Gómez-Ramos M, Moro AM. Binding-energy independence of reduced spectroscopic strengths derived from (p, 2p) and (p, pn) reactions with nitrogen and oxygen isotopes. Phys Lett B. 2018;785:511–6. Available from: https://doi.org/10.1016/j. physletb.2018.08.058.
- Phuc NT, Yoshida K, Ogata K. Toward a reliable description of (p, pN) reactions in the distorted-wave impulse approximation. Phys Rev C. 2019;100(6). Available from: https://doi.org/ 10.1103/PhysRevC.100.064604.